ATMOSPHERIC SCIENCE

Size-dependent influence of NO_x on the growth rates of organic aerosol particles

C. Yan[1*†], W. Nie[2*], A. L. Vogel[3,4‡], L. Dada[1], K. Lehtipalo[1,4,5†], D. Stolzenburg[6], R. Wagner[1], M. P. Rissanen[1], M. Xiao[4], L. Ahonen[1], L. Fischer[7], C. Rose[1§], F. Bianchi[1,8], H. Gordon[3,9‖], M. Simon[10], M. Heinritzi[10], O. Garmash[1], P. Roldin[11], A. Dias[3,12], P. Ye[13,14], V. Hofbauer[13], A. Amorim[12], P. S. Bauer[6], A. Bergen[10], A.-K. Bernhammer[7], M. Breitenlechner[7¶], S. Brilke[6,10], A. Buchholz[15], S. Buenrostro Mazon[1], M. R. Canagaratna[14], X. Chen[1#], A. Ding[2], J. Dommen[4], D. C. Draper[16], J. Duplissy[1], C. Frege[4], C. Heyn[4], R. Guida[3], J. Hakala[1], L. Heikkinen[1], C. R. Hoyle[4**], T. Jokinen[1], J. Kangasluoma[1,8], J. Kirkby[3,10], J. Kontkanen[1], A. Kürten[10], M. J. Lawler[16], H. Mai[17], S. Mathot[3], R. L. Mauldin III[13,18], U. Molteni[4], L. Nichman[19††], T. Nieminen[1], J. Nowak[14‡‡], A. Ojdanic[6], A. Onnela[3], A. Pajunoja[15], T. Petäjä[1,2], F. Piel[10§§], L. L. J. Quéléver[1], N. Sarnela[1], S. Schallhart[1‖‖], K. Sengupta[9], M. Sipilä[1], A. Tomé[20], J. Tröstl[4], O. Väisänen[15], A. C. Wagner[10¶¶], A. Ylisirniö[15], Q. Zha[1], U. Baltensperger[4], K. S. Carslaw[9], J. Curtius[10], R. C. Flagan[17], A. Hansel[1,7,21], I. Riipinen[22], J. N. Smith[16], A. Virtanen[15], P. M. Winkler[6], N. M. Donahue[13], V.-M. Kerminen[1], M. Kulmala[1,2,8,23], M. Ehn[1], D. R. Worsnop[1,14,15]

Atmospheric new-particle formation (NPF) affects climate by contributing to a large fraction of the cloud condensation nuclei (CCN). Highly oxygenated organic molecules (HOMs) drive the early particle growth and therefore substantially influence the survival of newly formed particles to CCN. Nitrogen oxide (NO_x) is known to suppress the NPF driven by HOMs, but the underlying mechanism remains largely unclear. Here, we examine the response of particle growth to the changes of HOM formation caused by NO_x. We show that NO_x suppresses particle growth in general, but the suppression is rather nonuniform and size dependent, which can be quantitatively explained by the shifted HOM volatility after adding NO_x. By illustrating how NO_x affects the early growth of new particles, a critical step of CCN formation, our results help provide a refined assessment of the potential climatic effects caused by the diverse changes of NO_x level in forest regions around the globe.

INTRODUCTION

Atmospheric new-particle formation (NPF) contributes to about half of the global tropospheric cloud condensation nuclei (CCN) population (*1*), thereby affecting Earth's radiation balance via aerosol-cloud interactions (*2*). However, considerable uncertainties exist on how atmospheric NPF and CCN production are associated with anthropogenic emissions of different aerosol precursor gases. The main reasons for these uncertainties are our incomplete knowledge on the mechanisms that dictate NPF and subsequent growth of newly formed particles to CCN sizes in the atmosphere.

[1]Institute for Atmospheric and Earth System Research/INAR–Physics, Faculty of Science, University of Helsinki, 00560 Helsinki, Finland. [2]Joint International Research Laboratory of Atmospheric and Earth System Sciences, School of Atmospheric Sciences, Nanjing University, Nanjing, China. [3]CERN, CH-1211, Geneva, Switzerland. [4]Laboratory of Atmospheric Chemistry, Paul Scherrer Institute, 5232 Villigen, Switzerland. [5]Finnish Meteorological Institute, Erik Palménin aukio 1, 00560 Helsinki, Finland. [6]University of Vienna, Faculty of Physics, Boltzmanngasse 5, 1090 Wien, Austria. [7]University of Innsbruck, Institute for Ion and Applied Physics, 6020 Innsbruck, Austria. [8]Aerosol and Haze Laboratory, Beijing Advanced Innovation Center for Soft Matter Science and Engineering, Beijing University of Chemical Technology, Beijing, China. [9]University of Leeds, Leeds LS2 9JT, UK. [10]Goethe University Frankfurt, Institute for Atmospheric and Environmental Sciences, Altenhöferallee 1, 60438 Frankfurt am Main, Germany. [11]Division of Nuclear Physics, Department of Physics, Lund University, P. O. Box 118, SE-221 00 Lund, Sweden. [12]CENTRA and FCUL, Universidade de Lisboa, Campo Grande, 1749-016 Lisboa, Portugal. [13]Carnegie Mellon University Center for Atmospheric Particle Studies, 5000 Forbes Ave., Pittsburgh, PA 15213, USA. [14]Aerodyne Research Inc., Billerica, MA 01821, USA. [15]University of Eastern Finland, Department of Applied Physics, P.O. Box 1627, 70211 Kuopio, Finland. [16]Department of Chemistry, University of California, Irvine, CA 92697, USA. [17]California Institute of Technology, 210-41, Pasadena, CA 91125, USA. [18]Department of Chemistry and Biochemistry, University of Colorado, Boulder, CO 80309, USA. [19]School of Earth and Environmental Science, University of Manchester, Manchester M13 9PL, UK [20]IDL Universidade da Beira Interior, Covilhã, Portugal. [21]IONICON GesmbH, Innsbruck, Austria. [22]Department of Environmental Science and Analytical Chemistry (ACES) and Bolin Centre for Climate Research, Stockholm University, 10691 Stockholm, Sweden. [23]Helsinki Institute of Physics, FI-00014 Helsinki, Finland.
*These authors contributed equally to this work.
†Corresponding author. Email: chao.yan@helsinki.fi (C.Y.); katrianne.lehtipalo@helsinki.fi (K.L.)
‡Present address: Institute for Atmospheric and Environmental Sciences, Goethe University Frankfurt, 60438 Frankfurt am Main, Germany.
§Present address: Université Clermont Auvergne, CNRS, Laboratoire de Météorologie Physique (LaMP), F-63000 Clermont-Ferrand, France.
‖Present address: Carnegie Mellon University, Forbes Avenue, Pittsburgh, PA 15213, USA.
¶Present address: Harvard University, 18 Oxford Street, Cambridge, MA 02138, USA.
#Present address: Institute of Physics, University of Tartu, W. Ostwaldi 1, EE-50411 Tartu, Estonia.
**Present address: Institute for Atmospheric and Climate Science, ETH Zurich, Switzerland.
††Present address: Flight Research Laboratory, National Research Council of Canada, Ottawa K1V 9B4, Canada.
‡‡Present address: NASA Langley Research Center, Hampton, VA 23681, USA.
§§Present address: Department of Chemistry, University of Oslo, 0315 Oslo, Norway.
‖‖Present address: Atmospheric Composition Research, Finnish Meteorological Institute, 00101 Helsinki, Finland.
¶¶ Present address: Department of Chemistry & CIRES, University of Colorado Boulder, 215 UCB, Boulder, CO 80309-0215, USA.

NPF consists of two consecutive steps: particle nucleation forming small clusters (usually 1 to 2 nm) and their further growth to larger sizes (*3*). The efficiencies of both steps together determine the rate of CCN formation from NPF: Particle nucleation produces an initial pool of newly formed particles, and these particles need to grow sufficiently fast to avoid being scavenged by the large preexisting particles (*4*). Organic vapors play crucial roles in both steps of NPF. Under most tropospheric conditions, particle nucleation is prevailingly driven by sulfuric acid (*3*, *5*), but organic vapors might act as an important stabilizing agent of sulfuric acid clusters (*6*, *7*). Organic vapors dominate particle growth in most tropospheric conditions (*8*, *9*) and therefore are crucial for the survival of newly formed particles.

The role of organic vapors in NPF differs significantly according to the volatility, which can span over 10 orders of magnitude (*10*). The formation and survival of newly formed particles are responsive to only a small fraction of organic vapors, which have (extremely) low volatility and thus are capable of clustering with themselves or sulfuric acid (*11*, *12*), and more readily condense onto the smallest particles and favor their survival from scavenging loss (*13*–*15*). Although observational evidence has suggested the existence of such low-volatility organic vapors (*15*), their identity and sources have been a puzzle for many years. Very recently, the autoxidation of peroxy radicals (RO_2), involving a few steps of intramolecular H migration and subsequent O_2 addition (*16*), has been found as the most efficient pathway of forming these low-volatility vapors (*17*). Chemically, these vapors are highly oxygenated and therefore are also widely referred to as highly oxygenated organic molecules (HOMs) (*18*).

Nitrogen oxides (NO_x), mainly emitted by anthropogenic activities nowadays, are key players in atmospheric chemistry through their reactions with other radicals (*19*). Their role in regulating atmospheric oxidants is well established (*20*, *21*), with a direct impact on volatile organic compound (VOC) oxidation processes and consequently on the formation of condensable organic vapors. NO_x has been found to significantly suppress NPF from monoterpene oxidation (*22*, *23*), although the cause was only speculated, lacking direct observations on a molecular level. As HOMs have been known as key precursors in NPF in multiple studies, it is foreseeable that investigating the influence of NO_x on them can help understand the details about this "NO_x suppression of particle formation." Two recent papers have addressed the role of NO_x on atmospheric autoxidation, suggesting that reduced NO_x concentrations will make autoxidation increasingly more important in the future (*24*), although the HOM formation rates from increased autoxidation may be counteracted by a concurrent decrease in oxidant concentrations (*25*). However, while these studies have addressed an overall "bulk" HOM formation potential, NO_x will affect not only the total HOM yield but also their composition and, thereby, their physical properties. Currently, our understanding of the effect of NO_x on particle formation can be improved from two aspects. First, the changes caused by NO_x on the chemical composition and bulk volatility of HOMs need to be understood based on direct measurement on a molecular level; second, the response of particle formation and growth to those changes in HOMs needs to be investigated in detail.

We conducted well-controlled NPF experiments using the CLOUD (Cosmics Leaving Outdoor Droplets) chamber equipped with a collection of state-of-the-art instruments. The comprehensive measurements allowed for obtaining important details of the NPF, from formation of low-volatility vapors to particle nucleation and further growth. After adding NO_x at levels up to only a few parts per billion by volume (ppbv), we observed substantial changes in both the growth rates (GRs) of new particles and HOM composition. We performed detailed analysis on HOM volatility based on their thermal desorption temperature and found that NO_x led to a significant increase of HOM volatilities, which, in turn, could be quantitatively connected to the suppression of particle GRs in a size-dependent manner.

RESULTS

We performed a set of experiments in the CLOUD chamber at CERN to investigate the effect of NO_x on particle formation via modifying the HOM composition. A typical experiment started with an injection of ozone and monoterpenes without any NO_x. A mixture of α-pinene and Δ-3-carene with 2:1 volume mixing ratio was used as VOC precursors to better resemble the monoterpene profile in a boreal forest station [SMEAR II (Station for Measuring Ecosystem-Atmosphere Relations)] in southern Finland (*26*). The ultraviolet (UV) system was kept on throughout the experiment which produces hydroxyl radicals (OH) by photolyzing O_3 (see Materials and Methods), in addition to those OH from ozonolysis of monoterpenes. These two sources together resulted in a steady-state OH concentration of around 10^6 cm^{-3}. Similar to previous CLOUD experiments (*12*), we started a typical experiment with adding monoterpene and ozone with zero ions in the chamber (referred to as neutral condition) and a relatively weak NPF occurred. We then turned off the high voltage [referred to as galactic cosmic ray (GCR) condition] and allowed the ions to trigger a stronger NPF that is distinguishable from the weaker one (see Fig. 1B). After the nucleation rate stabilized and particles grew to a few tens of nanometers, we injected NO into the chamber, which was oxidized mostly to NO_2 by O_3 (NO:NO_2 about 1%) and a small fraction further to NO_3 (NO_3:NO_x about 0.007%). As the NPF became progressively weaker when NO_x level increased, it is impossible to separate the subsequent weaker NPF case from the former stronger one. Therefore, when increasing the NO_x level, we also removed all ions for roughly 15 min (by turning on the high voltage) to quench the former nucleation, which resulted in a clear "gap" between the NPF cases (see Fig. 1B). The change of the HOM composition in both gas and particle phases as well as the particle dynamics were measured at three different NO_x concentration levels. Experiments with similar procedure were conducted with different monoterpene and SO_2 concentrations, except for experiment 1748, in which the "NPF gaps" were not inserted between NPF events, causing later events to be undistinguishable (see table S1). Other detailed information about the chamber operation and experimental conditions can be found in Materials and Methods.

NPF at different NO_x levels

We show in Fig. 1 one example of the resulting data (experiment 1752, see table S1), demonstrating the influence of NO_x on the HOM formation and NPF. A stepwise increase in the NO_x concentration caused an evident change in the HOM composition, featured by a large increase of the HOM monomer ($4 \leq$ carbon number ≤ 10) concentration and a simultaneous decrease of the HOM dimer ($10 <$ carbon number ≤ 20) concentration at higher NO_x concentrations (Fig. 1A). The monoterpene concentration did not change notably during the addition of NO_x, so the amount of monoterpenes available

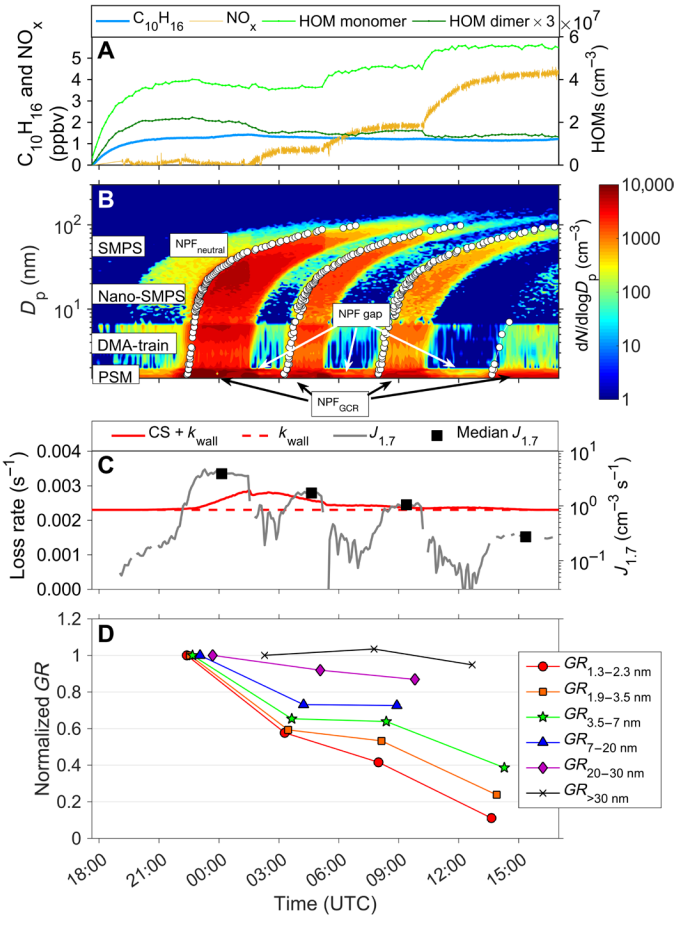

Fig. 1. Effect of NO_x addition on the formation and growth of particles. (**A**) Time series of monoterpenes ($C_{10}H_{16}$), NO_x, and HOM concentration. (**B**) Particle size distribution showing the four different NPF events detected under different NO_x conditions (0, 0.7, 1.9, and 4.5 ppbv). The appearance time of each particle size is marked by white dots, based on which we further determined the size-segregated GRs. (**C**) Temporal change of the nucleation rate at 1.7 nm ($J_{1.7}$) as well as the total loss rate (red solid line), which includes both the wall loss rate (red dashed line) and the condensation sink. (**D**) Normalized GRs at different size ranges. GRs at each specific size range are normalized to that measured under the zero NO_x condition, and the ratios represent the suppression by NO_x. It should be noted that such suppression degrees are only valid for this specific condition and will vary in other experiments (see fig. S1 and table S1).

for chemical reactions was roughly constant throughout the experiment. Some changes in the concentrations of oxidants were observed, but these changes were relatively small and cannot explain the observed major change in the HOM composition.

New particles were being formed continuously throughout the course of the experiment, where stronger bursts of new particles were observed for GCR conditions (see Supplementary Materials). We show in Fig. 1B that separated NPF events were triggered at different NO_x levels. We characterize these NPF events by their particle formation rate at 1.7 nm ($J_{1.7}$) and GRs in different size ranges (see the Supplementary Materials). As shown in our previous work, the nucleation in these experiments was driven by biogenic vapors (independent of H_2SO_4), and the large reduction of $J_{1.7}$ at higher NO_x levels (Fig. 1C) is a result of the decreased HOM dimer concentration (*11*).

We calculated the GRs of newly formed particles for different size ranges according to their appearance time into these sizes (see the Supplementary Materials). We found that the baseline GRs, measured at the zero NO_x condition, were 8.1 ± 4.5, 12.2 ± 4.7, 20.2 ± 3.7, 22.0 ± 0.9, 14.1 ± 0.6, and 10.6 ± 0.2 nm/hour in the size ranges of 1.3 to 2.3, 1.9 to 3.5, 3.5 to 7, 7 to 20, 20 to 30, and >30 nm, respectively. Size-segregated GRs after adding NO_x were also calculated and normalized to these baseline values (Fig. 1D). We found that the GRs at different size ranges were reduced by different degrees: The suppression was most pronounced for the smallest particles and increasingly weaker for larger ones, eventually becoming almost negligible for particles larger than 30 nm in diameter. These findings clearly indicate that the effect of NO_x cannot be thought of simply as an overall suppression on the full course of NPF, since otherwise, the GR at each size interval should have changed in the same way. Instead, the results suggest a more complicated change in the volatility distribution of condensable vapors.

We list size-segregated particle GRs determined for all experiments in table S1 and plot the normalized GRs in fig. S1. Experiments 1749 to 1752 were conducted with a high level of monoterpenes, and the strongest NPF events were observed in these experiments—the events were still distinguishable even when moderate-level NO_x was injected. However, reliable determination of particle GRs is challenging for experiments with lower monoterpene concentrations, e.g., experiments 1753 to 1755, when the NPF events were much weaker. The presence of H_2SO_4 led to less pronounced reduction of GRs, as the contribution of H_2SO_4 to particle growth was almost unaffected by NO_x. This can be seen by comparing experiments with similar monoterpene concentration but different H_2SO_4 concentration, e.g., experiments 1749 and 1752. We also noticed that there are some likely increase of $GR_{7\text{-}20\ nm}$ and $GR_{20\text{-}30\ nm}$ along with the increase of NO_x when H_2SO_4 is present (e.g., experiments 1749 and 1750; fig. S1). This indicates that H_2SO_4 may interact with HOMs on the surface of big particles, leading to an enhancement of HOM condensation. However, since the increase of GRs is not prominent (around 20% maximum) and is within the uncertainty range, it is difficult to fully validate this interpretation. For accuracy reasons, we use experiment 1752 as the best example to show the effect of NO_x, but overall, the size-dependent suppression on particle growth is evident in all experiments as long as the GRs can be well determined.

HOM composition modified by NO_x

We next investigate molecular-level changes in the HOM composition between conditions with and without NO_x, measured with a chemical ionization atmospheric-pressure-interface time-of-flight mass spectrometer (CI-APi-TOF, see Supplementary Materials). Changes in the HOM composition were observed immediately after NO_x was injected and were sensitive to the change of NO_x concentration (fig. S2). Here, we show the changes in HOM composition when 1.9 ppbv NO_x was added in comparison to that without NO_x. This condition is chosen as it better represents the typical NO_x level (about 1.5 ppbv) and also best resembles the HOM composition observed in a boreal forest station (SMEAR II) (fig. S2). To better describe the behavior of HOMs, in addition to the division of HOM monomers (marked with a subscript "mono") and dimers (subscript "di"), we further group them according to the number of contained nitrogen atoms (0, 1, or 2), which are marked with $C_xH_yO_z$, $C_xH_yO_zN$, and $C_xH_yO_zN_2$, respectively.

Before the injection of NO_x, the HOMs formed in our experiment were mostly $C_xH_yO_{z\_mono}$ (78.9%) and $C_xH_yO_{z\_di}$ (19.4%) compounds with a tiny fraction (1.7%) of residual $C_xH_yO_zN_{\_mono}$ compounds

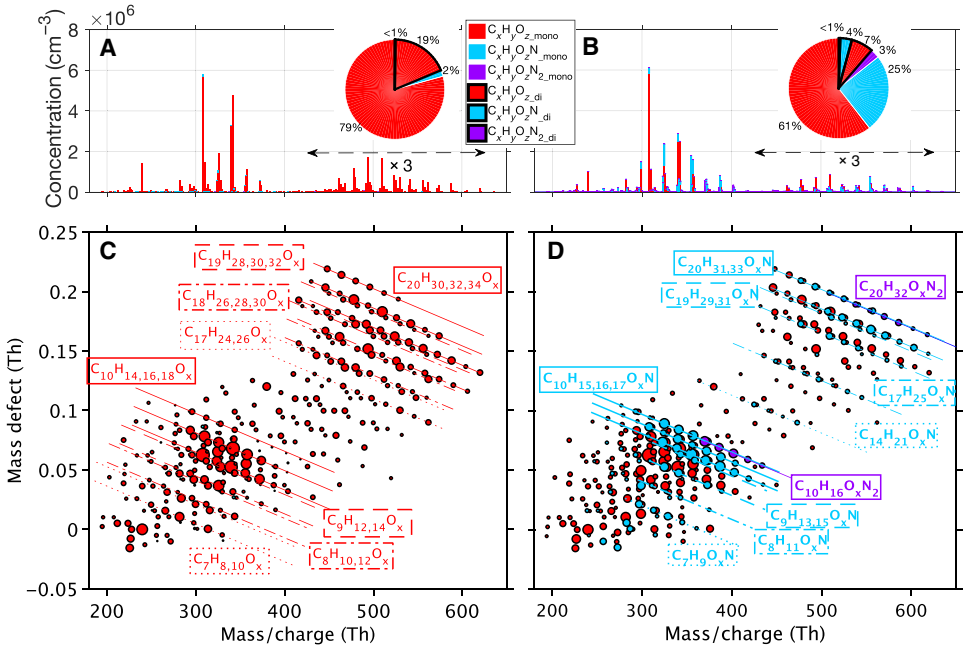

Fig. 2. Gas-phase HOMs under zero and 1.9 ppbv NO_x conditions measured by CI-APi-TOF in the CLOUD chamber. (**A** and **B**) The spectra of HOMs colored by their types. The pie charts give the fractional contribution of different types of HOMs. (**C** and **D**) Mass defect plots showing HOM composition under the two conditions. The *x* axis is the exact mass of HOMs, and the *y* axis is the mass defect. The color of circles denotes the type of HOMs, and their size is proportional to the logarithm of the count rate. Each straight line represents a group of compounds with the same number of carbon, hydrogen, and nitrogen but different numbers of oxygen atoms. The line style is the same as that used for the annotation frame.

left from the previous experiment (Fig. 2, A and C). The presence of 1.9 ppbv NO_x resulted in the formation of organic nitrates (Fig. 2, B and D), including $C_xH_yO_zN_{\_mono}$ (25.4%), $C_xH_yO_zN2_{\_mono}$ (3.0%), $C_xH_yO_zN_{\_di}$ (3.6%), and $C_xH_yO_zN2_{\_di}$ (0.5%). Meanwhile, $C_xH_yO_{z\_mono}$ and $C_xH_yO_{z\_di}$ decreased to 60.7 and 6.7%, respectively. The evolution of these species in the full course of the experiment can be seen in fig. S3.

The HOM formation is a result of several complicated reactions, in which the reactions between NO_x and RO_2 play an important role (*19*, *27*). We are not aiming to determine the exact contributions of all reaction pathways here, so instead, we summarize below the most important aspects of HOM formation and provide the supporting observational evidence in the Supplementary Materials. First, we found that the presence of NO_x had a small impact on the overall oxidative capacity in our experiments. Comparing conditions of 1.9 ppbv NO_x to zero NO_x, ozone and OH concentration decreased by about 3 and 10%, respectively. Some NO_3 radicals were also formed, as indicated by the presence of $C_xH_yO_zN_{1\text{-}2\_di}$ compounds (see the Supplementary Materials). Second, the reactions between NO and RO_2 were the main drivers of the changes in the HOM composition, i.e., the reduction of $C_xH_yO_{z\_di}$ and the formation of different $C_xH_yO_zN_{\_mono}$. However, a similar effect via the reaction between acylperoxy radical and NO_2 was also observed. Last, we did not observe HOMs containing sulfur, suggesting that SO_2 and H_2SO_4 were not directly involved in the HOM formation in the gas phase. The aforementioned main HOM formation pathways and the respective fingerprint molecules can be found in table S2.

In addition to the gas-phase HOMs, we also measured the particle-phase HOMs using the filter inlet for gases and aerosols (FIGAERO) coupled to an iodide-based chemical ionization time-of-flight mass spectrometer (see Supplementary Materials). The changes in the particle-phase HOM composition were generally similar to that of the gas-phase HOMs, featured by the increase of all types of organic nitrates and the decrease of non-nitrate HOMs, especially dimers ($C_xH_yO_{z\_di}$) (fig. S2). The simultaneous change of HOM composition in both gas and particle phases is a strong evidence that the particle formation is directly affected by condensation of gas-phase HOMs.

Change of HOM volatility distribution by NO_x

We finally estimate how the altered HOM composition changes the HOM volatility, a key parameter that governs HOM condensation and, therefore, connects the HOM chemistry with the particle growth behavior. We first investigated the HOM volatilities according to their thermal-desorption temperature (T_{max}, see the Supplementary Materials). Figure 3A shows the thermograms of three representative dimer compounds at different NO_x levels, i.e., $C_{19}H_{28}O_9$ (400.17 Th), $C_{20}H_{31}O_8N$ (413.20 Th), and $C_{20}H_{32}O_{11}N_2$ (476.20 Th), representing $C_xH_yO_{z\_di}$, $C_xH_yO_zN_{\_di}$, and $C_xH_yO_zN2_{\_di}$ compounds. Consistent with former observations of HOMs in the gas phase, along with the increase of NO_x, $C_{19}H_{28}O_9$ decreases in contrast to the increase of $C_{20}H_{31}O_8N$ and $C_{20}H_{32}O_{11}N_2$.

Although $C_{20}H_{32}O_{11}N_2$ has a higher molecular weight and a larger oxygen-to-carbon ratio (*O:C*) than $C_{19}H_{28}O_9$, it desorbs at a lower temperature, suggesting a higher volatility. Although the T_{max} of HOM dimers shows a weak dependence on the molecular weight (Fig. 3B), the large discrepancy of T_{max} between different types suggests that the molecular weight is not the most crucial parameter for their volatility. We found that T_{max} is strongly correlated with the effective *O:C* ($O{:}C_{eff}$) regardless of the HOM dimer type (Fig. 3C), indicating that $O{:}C_{eff}$ can be a good reference to their volatility. Here, the $O{:}C_{eff}$ is calculated based on the directly measured carbon and oxygen numbers but subtracting two oxygen atoms for each

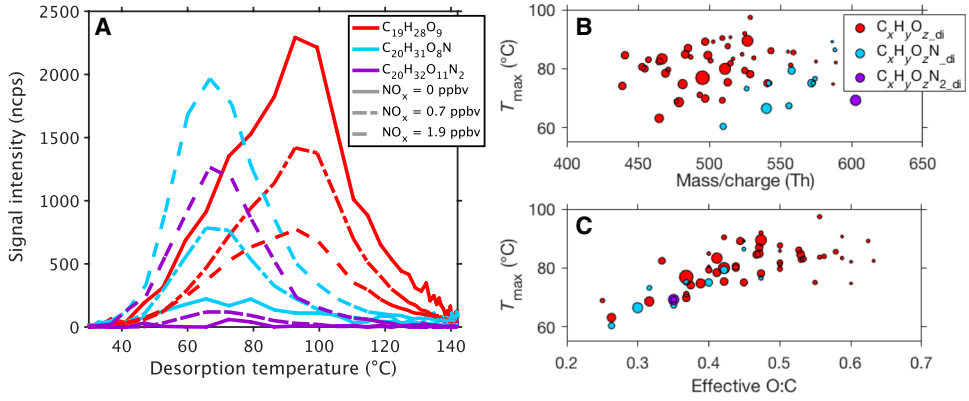

Fig. 3. Thermal desorption of particle-phase HOM dimers measured with the FIGAERO. (**A**) The thermogram of three example molecules under different NO_x conditions. Different line styles represent different NO_x conditions. The T_{max} is defined as the temperature at which the signal intensity reaches the maximum. (**B**) Correlation between T_{max} and mass-to-charge ratio for all HOM dimers. (**C**) Correlation between T_{max} and the effective O:C for all HOM dimers. The size of the circles in (B) and (C) is linearly proportional to the signal intensity of the desorption thermogram.

nitrogen atom. The use of $O{:}C_{eff}$ can be justified by the volatility dependence on the functional groups: It is suggested that the alcohol (-OH) and nitrate ($-ONO_2$) groups, contributing the same to $O{:}C_{eff}$, reduce the volatility by a comparable amount (*28*). The strong correlation between T_{max} and $O{:}C_{eff}$ was derived from the measurement of HOM dimers, as the observed T_{max} of HOM monomers often suffer from influences by the thermal decomposition of oligomeric compounds (*29*), which can be clearly seen in fig. S4. However, the fundamental assumption that the volatility is affected by functional groups should hold for monomers as well. Therefore, the relationship between T_{max} and volatility of monomers is expected to follow the same behavior. While we conclude that the influence of molecular weight on HOM volatility is minor when comparing different HOMs with similar carbon numbers, it becomes important for molecules containing very different numbers of carbon atoms, such as a HOM monomer versus a HOM dimer.

In our previous work, we parameterized the HOM volatility to the apparent $O{:}C$ (*14*), which is equal to the $O{:}C_{eff}$ for HOMs not containing nitrogen atoms. Here, we show that the same parameterization can be extended to other types of HOMs by simply replacing the apparent $O{:}C$ with the $O{:}C_{eff}$. The volatility of all types of HOMs in this study is thus estimated as $\log_{10}C^* = (0.672 - O{:}C_{eff})/0.078$ and $\log_{10}C^* = (0.209 - O{:}C_{eff})/0.052$ for HOM monomers and dimers, respectively.

After applying the volatility parameterization to all HOMs, we can obtain the overall HOM volatility distribution by grouping them into volatility bins. For simplicity, we compare the volatility distribution at zero NO_x and 1.9 ppbv NO_x (Fig. 4A). In both cases, the volatility spans a large range from extremely low-volatility organic compounds (ELVOCs, $C^* \leq 10^{-4.5}$ μg m^{-3} or roughly equivalent to $N^* \leq 5 \times 10^4$ cm^{-3} assuming an average molar mass of 300 Da), through low-volatility organic compounds (LVOCs, $10^{-4.5} < C^* \leq 10^{-0.5}$ μg m^{-3}; $5 \times 10^4 < N^* \leq 5 \times 10^8$ cm^{-3}), and on to semivolatile organic compounds (SVOCs, $10^{-0.5} < C^* \leq 10^{2.5}$ μg m^{-3} or $5 \times 10^8 < N^* \leq 5 \times 10^{11}$ cm^{-3}). Adding NO_x considerably shifts the overall distribution toward a higher volatility. As shown in fig. S5, the fractional decrease of ELVOCs is mostly due to the suppressed $C_xH_yO_{z\_di}$ formation by NO_x, which is slightly compensated by the formation of $C_xH_yO_zN_{1\text{-}2\_di}$. The increase of LVOCs and SVOCs mostly results from the formation of $C_xH_yO_zN_{1\text{-}2\_mono}$. Simply put, NO_x suppresses dimer formation and replaces dimers with organic nitrate monomers.

Since the particle GR depends approximately linearly on the concentration of condensable vapors, the ratio of particle GRs at different NO_x conditions shown in Fig. 1 should be reflective of the corresponding HOM concentration ratios. Figure 4B shows the cumulative HOM concentrations for the two NO_x conditions together with their ratio, which increases from ~0.2 for the nonvolatile HOMs ($C^* \leq 10^{-15}$ μg m^{-3} or $N^* \ll 1$ cm^{-3}) close to unity when counting all LVOCs ($C^* < 10^{-0.5}$ μg m^{-3} or 5×10^8 cm^{-3}). This volatility measurement, relying on the identity and T_{max} of HOMs, provides the confirmation of our initial hypothesis that the change in HOM composition caused by NO_x is indeed able to explain the observed size-dependent GRs: The abundance of the least volatile vapors is substantially reduced, thus affecting the growth of the smallest particles, while the total concentration of vapors able to condense onto particles with diameters of a few tens of nanometers remains similar.

The tight connection between HOM volatility and particle formation is also supported by the correlogram between the cumulative HOM concentration and particle formation and GRs using data from all experiments listed in table S1. As shown in fig. S6, the correlation coefficient for $GR_{1.9\text{-}3.5\ nm}$ is at maximum for HOMs with $C^* \leq 10^{-7.5}$ μg m^{-3} ($N^* \leq 5 \times 10^1$ cm^{-3}), and quickly decreases if HOMs of higher volatility are included, indicating that these higher-volatility HOMs do not contribute to the particle growth in this size range. Such quick decline of the correlation coefficient for the $GR_{20\text{-}30\ nm}$ only occurs when HOMs of $C^* \geq 10^{-2.5}$ μg m^{-3} ($N^* \geq 5 \times 10^6$ cm^{-3}) are counted, showing a less strict volatility requirement for growing 20- to 30-nm particles owing to the diminished curvature effect. Moreover, the correlations for $J_{1.7}$ and $GR_{1.9\text{-}3.5\ nm}$ show very similar patterns, suggesting that the formation and growth of particles at these size ranges are likely led by the same vapors or at least by vapors with nearly fixed relative yields.

DISCUSSION

In summary, using the CERN CLOUD facilities, we performed dedicated experiments to investigate the role of NO_x in the particle growth under conditions that mimic the atmosphere in a boreal forest

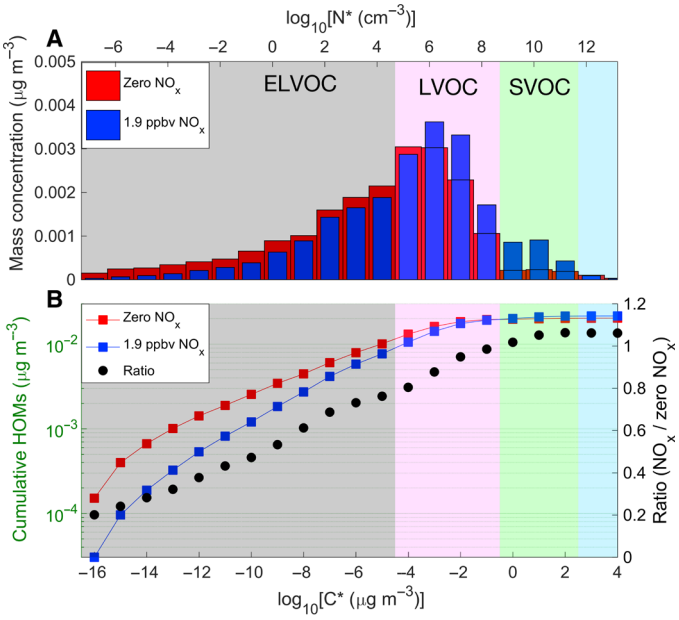

Fig. 4. Volatility distribution of gas-phase HOMs under zero and 1.9 ppbv NO_x conditions. (**A**) The summed HOM concentrations of each bin. (**B**) The cumulative HOM concentrations. Red and blue markers denote HOM concentrations under zero and 1.9 ppbv NO_x, respectively. The black dots give the ratio of cumulative concentrations of $[HOM]_{NOx}$:$[HOM]_{w/o\ NOx}$.

with slight influence by human activities. The comprehensive measurements of both the particle precursors vapors (HOMs) and the particle dynamics allow us to evaluate the influence of NO_x at all stages of gas-to-particle conversion—from the oxidation of VOC forming HOMs to the particle nucleation and the subsequent particle growth over various size ranges. Our results show a generally consistent picture with the few recent studies that NPF is suppressed by NO_x due to the change of HOM chemistry (*22*, *23*). However, on the basis of the detailed analysis on particle dynamics, we reveal that the suppression effect of NO_x on particle formation is rather nonuniform and size dependent. Furthermore, we elucidate that the size-dependent suppression on particle growth can be quantitatively connected to the increased HOM bulk volatility as a result of changes in the HOM chemistry and composition.

In our experiments, we also observed suppressed particle formation rates ($J_{1.7}$) and attributed this to the reduced HOM dimer formation (*11*). However, this effect becomes significantly weaker when also NH_3 and H_2SO_4 are present (*11*). This means that the suppression effect of NO_x on particle nucleation, reported in previous studies (*22*, *23*) and in this work, cannot be directly applied to the atmosphere where NH_3 or even stronger bases together with H_2SO_4 tend to drive the nucleation.

However, unlike the particle nucleation, the suppression of particle growth driven by HOMs is directly relevant to the ambient atmosphere. After adding NO_x, we observed much stronger influence (suppression) on particle growth of small particles (~2 nm), while that on large particles (>30 nm) was negligible. This observation has important implications. First, as smaller particles are more easily scavenged by preexisting particles, the attenuated GR of small particles significantly reduces the survival probability of the newly formed particles and thus causes a reduction of the concentration of CCN-size particles, as seen in our experiments. Second, it also provides a plausible explanation for the laboratory observations showing that NO_x has a smaller effect on the yield regarding secondary organic aerosol (SOA) formation than on NPF (*22*, *23*). In addition, our results show that NO is more effective than NO_2 in changing the HOM composition and volatility. This indicates that, besides the commonly used term "VOC/NO_x," the NO:NO_2 ratio is another crucial parameter in understanding the influence of NO_x on SOA formation.

From a more general perspective, our results contribute to the understanding on the climatic effects of NO_x. It is well known that NO_x can form inorganic nitrate aerosol via HNO_3 condensation and reactive uptake of N_2O_5 (*30*) and contribute to the formation of organic nitrate aerosol via the NO_3-initiated oxidation (*31*). The nitrate constituents are able to modify several aerosol properties, including their hygroscopicity (*32*) and light absorption capability (*33*). Our results suggest that in monoterpene-rich environments, such as forested areas, NO_x can significantly reduce the CCN formation and thereby influence cloud properties. Our experimental insights, as presented above, can also help improve the modeling of such effects.

MATERIALS AND METHODS

The CLOUD facility

The CLOUD chamber is a stainless steel cylinder with a volume of ca. 26.1 m^3, located at CERN, Geneva, Switzerland. The most important feature of this chamber is its ultracleanliness, which allows one to study the NPF phenomenon under carefully controlled and atmospherically relevant conditions, i.e., with precursors of similar concentrations to those in the atmosphere. Dedicated efforts are made to ensure a low contamination level in the chamber; besides the electropolished inner surfaces of the chamber, vigorous rinsing with ultrapure water at 373 K is done before each campaign, and ultraclean synthetic air produced by mixing cryogenic liquid nitrogen and oxygen is used throughout the experiments. The background total VOC concentration is at sub-ppbv level, and the total condensable vapor concentration is at sub-pptv (parts per trillion by volume) level. Ion concentrations in the chamber can be controlled with a high-voltage clearing field. By turning on the high-voltage field (20 kV m^{-1}), all ions and charged particles are removed; we refer to this as the neutral condition state. When the high voltage is switched off, ions are produced by the GCR in the chamber; we refer to this as the GCR condition.

To mimic the photochemistry caused by sunlight in the atmosphere, a UV light system was used. The system consists of three light sources that cover different regions of the UV and visible spectrum. A krypton fluoride excimer UV laser (3 W, λ = 248 nm) is used to produce OH via O_3 photolysis. Two UV light-emitting diodes (LEDs; 2 × 16.5 W, λ = 370 to 390 nm) are used to photolyze NO_2 into NO. In addition, four Hamamatsu Xenon arc lamps (4 × 200 W, λ = 250 to 580 nm) are used to provide broad range UV light and bring the overall UV spectrum closer to atmospheric levels. The xenon arc light and the UV laser are fed vertically through the top of the chamber by optical fibers, while the UV LEDs shine into the chamber horizontally from opposite sides in the middle plane. All gases are injected through a dedicated inlet system from the bottom of the chamber. In order to improve the homogeneity of gas mixing inside the big chamber volume, two mixing fans are mounted on the top and the bottom of the chamber.

Experimental design

We conducted a set of experiments for studying the effect of NO_x on HOM production and NPF at constant temperature (278 K) and relative humidity (38%). We kept the injection rate of ozone constant throughout the experiments, thereby maintaining an ozone volume mixing ratio of ca. 40 ppbv. We started a typical experiment with adding monoterpenes under neutral conditions. The monoterpene precursors were a mix of α-pinene and Δ-3-carene, the two most abundant monoterpenes at the Hyytiälä station with an initial mixing ratio of 2:1 (*26*); these compounds are structurally similar, both having one endocyclic double bond on the six-carbon ring. Once the HOM concentration reached steady state and the nucleation rate also stabilized, we turned off the high voltage and allowed the ion concentration to build up, which is referred to in CLOUD experiments as the GCR condition. The ions triggered a stronger particle nucleation that can be easily distinguished from the previous, weaker one under neutral conditions. After the nucleation rate at the GCR condition reached the plateau and the particles grew to a few tens of nanometers, we started injecting NO into the chamber, most of which is quickly oxidized to NO_2 by O_3; a small fraction of the NO_2 can be further oxidized to NO_3. The injection rate of NO was equivalent to a photolysis rate J_{NO2} of 1.5×10^{-4} s^{-1}, about one order of magnitude lower than that at the Hyytiälä station in spring daytime (median value of 2.7×10^{-3} s^{-1}). As a result, the final NO:NO_2 was at ca. 1%, lower than in the atmosphere at our reference station. After all types of HOMs reached steady state and a stable nucleation rate was obtained, the NO_x level was further increased. In most of the experiments, we increased NO_x in three stages: ~0.7, 1.9, and 4.5 ppbv NO_x. Because each step of increasing NO_x led to a weaker NPF event, we activated the clearing field for about 15 min to quench the previous NPF event, thereby separating the new nucleation event from the previous one for better characterization. We refer the aforementioned experimental sequence as one complete run, which was repeated with various initial monoterpene concentrations coupled with different initial SO_2 concentrations. Throughout the run, the UV light system was kept on to avoid any change in NPF associated to a varied UV irradiation. The main experimental variables are listed in table S1.

We monitored the NPF events with a variety of instruments (see the Supplementary Materials) and calculated size-resolved particle GRs according to their appearance time (see the Supplementary Materials and fig.S6). In addition, we deployed two chemical ionization mass spectrometers (CIMS) to extend observations of NPF into a molecular level: a nitrate-based CIMS, also known as CI-APi-TOF, for measuring sulfuric acid and more oxidized HOMs in the gas phase and an iodide-based CIMS equipped with FIGAERO focusing on detecting oxidation products of VOCs in the particle phase (see the Supplementary Materials). We estimated the HOM volatility from their thermal desorption temperature (T_{max}) together with the volatility parameterization developed by Tröstl and co-workers (*14*).

SUPPLEMENTARY MATERIALS

Supplementary material for this article is available at http://advances.sciencemag.org/cgi/content/full/6/22/eaay4945/DC1

REFERENCES AND NOTES

1. J. Merikanto, D. V. Spracklen, G. W. Mann, S. J. Pickering, K. S. Carslaw, Impact of nucleation on global CCN. *Atmos. Chem. Phys.* **9**, 8601–8616 (2009).
2. O. Boucher, D. Randall, P. Artaxo, C. Bretherton, G. Feingold, P. Forster, V.-M. Kerminen, Y. Kondo, H. Liao, U. Lohmann, P. Rasch, S. K. Satheesh, S. Sherwood, B. Stevens, X. Y. Zhang, *Climate Change 2013: The Physical Science Basis. Contribution of Working Group I to the Fifth Assessment Report of the Intergovernmental Panel on Climate Change* (Cambridge Univ. Press, 2013), pp. 571–657.
3. M. Kulmala, J. Kontkanen, H. Junninen, K. Lehtipalo, H. E. Manninen, T. Nieminen, T. Petäjä, M. Sipilä, S. Schobesberger, P. Rantala, A. Franchin, T. Jokinen, E. Järvinen, M. Äijälä, J. Kangasluoma, J. Hakala, P. P. Aalto, P. Paasonen, J. Mikkilä, J. Vanhanen, J. Aalto, H. Hakola, U. Makkonen, T. Ruuskanen, R. L. Mauldin III, J. Duplissy, H. Vehkamäki, J. Bäck, A. Kortelainen, I. Riipinen, T. Kurtén, M. V. Johnston, J. N. Smith, M. Ehn, T. F. Mentel, K. E. J. Lehtinen, A. Laaksonen, V.-M. Kerminen, D. R. Worsnop, Direct observations of atmospheric aerosol nucleation. *Science* **339**, 943–946 (2013).
4. H. Vehkamäki, I. Riipinen, Thermodynamics and kinetics of atmospheric aerosol particle formation and growth. *Chem. Soc. Rev.* **41**, 5160–5173 (2012).
5. P. H. Mcmurry, M. Fink, H. Sakurai, M. R. Stolzenburg, R. L. Mauldin III, J. Smith, F. Eisele, K. Moore, S. Sjostedt, D. Tanner, L. G. Huey, J. B. Nowak, E. Edgerton, D. Voisin, A criterion for new particle formation in the sulfur–rich Atlanta atmosphere. *J. Geophys. Res. Atmos.* **110**, 2935–2948 (2005).
6. F. Riccobono, S. Schobesberger, C. E. Scott, J. Dommen, I. K. Ortega, L. Rondo, J. Almeida, A. Amorim, F. Bianchi, M. Breitenlechner, A. David, A. Downard, E. M. Dunne, J. Duplissy, S. Ehrhart, R. C. Flagan, A. Franchin, A. Hansel, H. Junninen, M. Kajos, H. Keskinen, A. Kupc, A. Kürten, A. N. Kvashin, A. Laaksonen, K. Lehtipalo, V. Makhmutov, S. Mathot, T. Nieminen, A. Onnela, T. Petäjä, A. P. Praplan, F. D. Santos, S. Schallhart, J. H. Seinfeld, M. Sipilä, D. V. Spracklen, Y. Stozhkov, F. Stratmann, A. Tomé, G. Tsagkogeorgas, P. Vaattovaara, Y. Viisanen, A. Vrtala, P. E. Wagner, E. Weingartner, H. Wex, D. Wimmer, K. S. Carslaw, J. Curtius, N. M. Donahue, J. Kirkby, M. Kulmala, D. R. Worsnop, U. Baltensperger, Oxidation products of biogenic emissions contribute to nucleation of atmospheric particles. *Science* **344**, 717–721 (2014).
7. R. Zhang, I. Suh, J. Zhao, D. Zhang, E. C. Fortner, X. Tie, L. T. Molina, M. J. Molina, Atmospheric new particle formation enhanced by organic acids. *Science* **304**, 1487–1490 (2004).
8. I. Riipinen, J. R. Pierce, T. Yli-Juuti, T. Nieminen, S. Häkkinen, M. Ehn, H. Junninen, K. Lehtipalo, T. Petäjä, J. Slowik, R. Chang, N. C. Shantz, J. Abbatt, W. R. Leaitch, V.-M. Kerminen, D.-R. Worsnop, S. N. Pandis, N. M. Donahue, M. Kulmala, Organic condensation: A vital link connecting aerosol formation to cloud condensation nuclei (CCN) concentrations. *Atmos. Chem. Phys.* **11**, 3865–3878 (2011).
9. J. N. Smith, M. J. Dunn, T. M. Van Reken, K. Iida, M. R. Stolzenburg, P. H. McMurry, L. G. Huey, Chemical composition of atmospheric nanoparticles formed from nucleation in Tecamac, Mexico: Evidence for an important role for organic species in nanoparticle growth. *Geophys. Res. Lett.* **35**, 228–236 (2008).
10. N. M. Donahue, J. H. Kroll, S. N. Pandis, A. L. Robinson, A two-dimensional volatility basis set—Part 2: Diagnostics of organic-aerosol evolution. *Atmos. Chem. Phys.* **12**, 615–634 (2012).
11. K. Lehtipalo, C. Yan, L. Dada, F. Bianchi, M. Xiao, R. Wagner, D. Stolzenburg, L. R. Ahonen, A. Amorim, A. Baccarini, P. S. Bauer, B. Baumgartner, A. Bergen, A.-K. Bernhammer, M. Breitenlechner, S. Brilke, A. Buchholz, S. B. Mazon, D. Chen, X. Chen, A. Dias, J. Dommen, D. C. Draper, J. Duplissy, M. Ehn, H. Finkenzeller, L. Fischer, C. Frege, C. Fuchs, O. Garmash, H. Gordon, J. Hakala, X. He, L. Heikkinen, M. Heinritzi, J. C. Helm, V. Hofbauer, C. R. Hoyle, T. Jokinen, J. Kangasluoma, V.-M. Kerminen, C. Kim, J. Kirkby, J. Kontkanen, A. Kürten, M. J. Lawler, H. Mai, S. Mathot, R. L. Mauldin III, U. Molteni, L. Nichman, W. Nie, T. Nieminen, A. Ojdanic, A. Onnela, M. Passananti, T. Petäjä, F. Piel, V. Pospisilova, L. L. J. Quéléver, M. P. Rissanen, C. Rose, N. Sarnela, S. Schallhart, S. Schuchmann, K. Sengupta, M. Simon, M. Sipilä, C. Tauber, A. Tomé, J. Tröstl, O. Väisänen, A. L. Vogel, R. Volkamer, A. C. Wagner, M. Wang, L. Weitz, D. Wimmer, P. Ye, A. Ylisirniö, Q. Zha, K. S. Carslaw, J. Curtius, N. M. Donahue, R. C. Flagan, A. Hansel, I. Riipinen, A. Virtanen, P. M. Winkler, U. Baltensperger, M. Kulmala, D. R. Worsnop, Multicomponent new particle formation from sulfuric acid, ammonia, and biogenic vapors. *Sci. Adv.* **4**, eaau5363 (2018).
12. J. Kirkby, J. Duplissy, K. Sengupta, C. Frege, H. Gordon, C. Williamson, M. Heinritzi, M. Simon, C. Yan, J. Almeida, J. Tröstl, T. Nieminen, I. K. Ortega, R. Wagner, A. Adamov, A. Amorim, A.-K. Bernhammer, F. Bianchi, M. Breitenlechner, S. Brilke, X. Chen, J. Craven, A. Dias, S. Ehrhart, R. C. Flagan, A. Franchin, C. Fuchs, R. Guida, J. Hakala, C. R. Hoyle, T. Jokinen, H. Junninen, J. Kangasluoma, J. Kim, M. Krapf, A. Kürten, A. Laaksonen, K. Lehtipalo, V. Makhmutov, S. Mathot, U. Molteni, A. Onnela, O. Peräkylä, F. Piel, T. Petäjä, A. P. Praplan, K. Pringle, A. Rap, N. A. D. Richards, I. Riipinen, M. P. Rissanen, L. Rondo, N. Sarnela, S. Schobesberger, C. E. Scott, J. H. Seinfeld, M. Sipilä, G. Steiner, Y. Stozhkov, F. Stratmann, A. Tomé, A. Virtanen, A. L. Vogel, A. C. Wagner, P. E. Wagner, E. Weingartner, D. Wimmer, P. M. Winkler, P. Ye, X. Zhang, A. Hansel, J. Dommen, N. M. Donahue, D. R. Worsnop, U. Baltensperger, M. Kulmala, K. S. Carslaw, J. Curtius, Ion-induced nucleation of pure biogenic particles. *Nature* **533**, 521–526 (2016).
13. N. M. Donahue, I. K. Ortega, W. Chuang, I. Riipinen, F. Riccobono, S. Schobesberger, J. Dommen, U. Baltensperger, M. Kulmala, D. R. Worsnop, H. Vehkamaki, How do organic vapors contribute to new-particle formation? *Faraday Discuss.* **165**, 91–104 (2013).
14. J. Tröstl, W. K. Chuang, H. Gordon, M. Heinritzi, C. Yan, U. Molteni, L. Ahlm, C. Frege, F. Bianchi, R. Wagner, M. Simon, K. Lehtipalo, C. Williamson, J. S. Craven, J. Duplissy,

A. Adamov, J. Almeida, A.-K. Bernhammer, M. Breitenlechner, S. Brilke, A. Dias, S. Ehrhart, R. C. Flagan, A. Franchin, C. Fuchs, R. Guida, M. Gysel, A. Hansel, C. R. Hoyle, T. Jokinen, H. Junninen, J. Kangasluoma, H. Keskinen, J. Kim, M. Krapf, A. Kürten, A. Laaksonen, M. Lawler, M. Leiminger, S. Mathot, O. Möhler, T. Nieminen, A. Onnela, T. Petäjä, F. M. Piel, P. Miettinen, M. P. Rissanen, L. Rondo, N. Sarnela, S. Schobesberger, K. Sengupta, M. Sipilä, J. N. Smith, G. Steiner, A. Tomè, A. Virtanen, A. C. Wagner, E. Weingartner, D. Wimmer, P. M. Winkler, P. Ye, K. S. Carslaw, J. Curtius, J. Dommen, J. Kirkby, M. Kulmala, I. Riipinen, D. R. Worsnop, N. M. Donahue, U. Baltensperger, The role of low-volatility organic compounds in initial particle growth in the atmosphere. *Nature* **533**, 527–531 (2016).

15. I. Riipinen, T. Yli-Juuti, J. R. Pierce, T. Petäjä, D. R. Worsnop, M. Kulmala, N. M. Donahue, The contribution of organics to atmospheric nanoparticle growth. *Nat. Geosci.* **5**, 453–458 (2012).
16. J. D. Crounse, L. B. Nielsen, S. Jørgensen, H. G. Kjaergaard, P. O. Wennberg, Autoxidation of organic compounds in the atmosphere. *J. Phys. Chem. Lett.* **4**, 3513–3520 (2013).
17. M. Ehn, J. A. Thornton, E. Kleist, M. Sipilä, H. Junninen, I. Pullinen, M. Springer, F. Rubach, R. Tillmann, B. Lee, F. Lopez-Hilfiker, S. Andres, I.-H. Acir, M. Rissanen, T. Jokinen, S. Schobesberger, J. Kangasluoma, J. Kontkanen, T. Nieminen, T. Kurtén, L. B. Nielsen, S. Jørgensen, H. G. Kjaergaard, M. Canagaratna, M. D. Maso, T. Berndt, T. Petäjä, A. Wahner, V.-M. Kerminen, M. Kulmala, D. R. Worsnop, J. Wildt, T. F. Mentel, A large source of low-volatility secondary organic aerosol. *Nature* **506**, 476–479 (2014).
18. M. Ehn, E. Kleist, H. Junninen, T. Petäjä, G. Lönn, S. Schobesberger, M. Dal Maso, A. Trimborn, M. Kulmala, D. R. Worsnop, A. Wahner, J. Wildt, T. F. Mentel, Gas phase formation of extremely oxidized pinene reaction products in chamber and ambient air. *Atmos. Chem. Phys.* **12**, 5113–5127 (2012).
19. J. J. Orlando, G. S. Tyndall, Laboratory studies of organic peroxy radical chemistry: An overview with emphasis on recent issues of atmospheric significance. *Chem. Soc. Rev.* **41**, 6294–6317 (2012).
20. J. H. Seinfeld, S. N. Pandis, *Atmospheric Chemistry and Physics: From Air Pollution to Climate Change* (John Wiley & Sons, 2012).
21. B. J. Finlayson-Pitts, J. N. Pitts Jr., *Atmospheric Chemistry: Fundamentals and Experimental Techniques* (Wiley, 1986).
22. J. Wildt, T. F. Mentel, A. Kiendler-Scharr, T. Hoffmann, S. Andres, M. Ehn, E. Kleist, P. Müsgen, F. Rohrer, Y. Rudich, M. Springer, R. Tillmann, A. Wahner, Suppression of new particle formation from monoterpene oxidation by NO_x. *Atmos. Chem. Phys.* **14**, 2789–2804 (2014).
23. D. Zhao, S. H. Schmitt, M. Wang, I.-H. Acir, R. Tillmann, Z. Tan, A. Novelli, H. Fuchs, I. Pullinen, R. Wegener, F. Rohrer, J. Wildt, A. Kiendler-Scharr, A. Wahner, T. F. Mentel, Effects of NO_x and SO_2 on the secondary organic aerosol formation from photooxidation of α-pinene and limonene. *Atmos. Chem. Phys.* **18**, 1611–1628 (2018).
24. E. Praske, R. V. Otkjær, J. D. Crounse, J. C. Hethcox, B. M. Stoltz, H. G. Kjaergaard, P. O. Wennberg, Atmospheric autoxidation is increasingly important in urban and suburban North America. *Proc. Natl. Acad. Sci. U.S.A.* **115**, 64–69 (2018).
25. H. O. Pye, E. L. D'Ambro, B. H. Lee, S. Schobesberger, M. Takeuchi, Y. Zhao, F. Lopez-Hilfiker, J. Liu, J. E. Shilling, J. Xing, R. Mathur, A. M. Middlebrook, J. Liao, A. Welti, M. Graus, C. Warneke, J. A. de Gouw, J. S. Holloway, T. B. Ryerson, I. B. Pollack, J. A. Thornton, Anthropogenic enhancements to production of highly oxygenated molecules from autoxidation. *Proc. Natl. Acad. Sci. U.S.A.* **116**, 6641–6646 (2019).
26. J. Rinne, H. Hakola, T. Laurila, Ü. Rannik, Canopy scale monoterpene emissions of *Pinus sylvestris* dominated forests. *Atmos. Environ.* **34**, 1099–1107 (2000).
27. F. Bianchi, T. Kurtén, M. Riva, C. Mohr, M. P. Rissanen, P. Roldin, T. Berndt, J. D. Crounse, P. O. Wennberg, T. F. Mentel, J. Wildt, H. Junninen, T. Jokinen, M. Kulmala, D. R. Worsnop, J. A. Thornton, N. Donahue, H. G. Kjaergaard, M. Ehn, Highly oxygenated organic molecules (HOM) from gas-phase autoxidation involving peroxy radicals: A key contributor to atmospheric aerosol. *Chem. Rev.* **119**, 3472–3509 (2019).
28. W. K. Chuang, N. M. Donahue, A two-dimensional volatility basis set—Part 3: Prognostic modeling and NO_x dependence. *Atmos. Chem. Phys.* **16**, 123–134 (2016).
29. H. Stark, R. L. N. Yatavelli, S. L. Thompson, H. Kang, J. E. Krechmer, J. R. Kimmel, B. B. Palm, W. Hu, P. L. Hayes, D. A. Day, P. Campuzano-Jost, M. R. Canagaratna, J. T. Jayne, D. R. Worsnop, J. L. Jimenez, Impact of thermal decomposition on thermal desorption instruments: Advantage of thermogram analysis for quantifying volatility distributions of organic species. *Environ. Sci. Technol.* **51**, 8491–8500 (2017).
30. H. Wang, K. Lu, X. Chen, Q. Zhu, Q. Chen, S. Guo, M. Jiang, X. Li, D. Shang, Z. Tan, Y. Wu, Z. Wu, Q. Zou, Y. Zheng, L. Zeng, T. Zhu, M. Hu, Y. Zhang, High N_2O_5 concentrations observed in urban Beijing: Implications of a large nitrate formation pathway. *Environ. Sci. Technol. Lett.* **4**, 416–420 (2017).
31. A. Kiendler-Scharr, A. A. Mensah, E. Friese, D. Topping, E. Nemitz, A. S. H. Prevot, M. Äijälä, J. Allan, F. Canonaco, M. Canagaratna, S. Carbone, M. Crippa, M. Dall Osto, D. A. Day, P. De Carlo, C. F. Di Marco, H. Elbern, A. Eriksson, E. Freney, L. Hao, H. Herrmann, L. Hildebrandt, R. Hillamo, J. L. Jimenez, A. Laaksonen, G. McFiggans, C. Mohr, C. O'Dowd, R. Otjes, J. Ovadnevaite, S. N. Pandis, L. Poulain, P. Schlag, K. Sellegri, E. Swietlicki, P. Tiitta, A. Vermeulen, A. Wahner, D. Worsnop, H.-C. Wu, Ubiquity of organic nitrates from nighttime chemistry in the European submicron aerosol. *Geophys. Res. Lett.* **43**, 7735–7744 (2016).
32. M. H. Barley, D. Topping, D. Lowe, S. Utembe, G. McFiggans, The sensitivity of secondary organic aerosol (SOA) component partitioning to the predictions of component properties—Part 3: Investigation of condensed compounds generated by a near-explicit model of VOC oxidation. *Atmos. Chem. Phys.* **11**, 13145–13159 (2011).
33. T. Moise, J. M. Flores, Y. Rudich, Optical properties of secondary organic aerosols and their changes by chemical processes. *Chem. Rev.* **115**, 4400–4439 (2015).
34. T. Jokinen, T. Berndt, R. Makkonen, V.-M. Kerminen, H. Junninen, P. Paasonen, F. Stratmann, H. Herrmann, A. B. Guenther, D. R. Worsnop, M. Kulmala, M. Ehn, M. Sipilä, Production of extremely low volatile organic compounds from biogenic emissions: Measured yields and atmospheric implications. *Proc. Natl. Acad. Sci. U.S.A.* **112**, 7123–7128 (2015).
35. T. Jokinen, M. Sipilä, H. Junninen, M. Ehn, G. Lönn, J. Hakala, T. Petäjä, R. L. Mauldin III, M. Kulmala, D. R. Worsnop, Atmospheric sulphuric acid and neutral cluster measurements using CI-APi-TOF. *Atmos. Chem. Phys.* **12**, 4117–4125 (2012).
36. H. Junninen, M. Ehn, T. Petäjä, L. Luosujärvi, T. Kotiaho, R. Kostiainen, U. Rohner, M. Gonin, K. Fuhrer, M. Kulmala, D. R. Worsnop, A high-resolution mass spectrometer to measure atmospheric ion composition. *Atmos. Meas. Tech.* **3**, 1039–1053 (2010).
37. M. Heinritzi, M. Simon, G. Steiner, A. C. Wagner, A. Kürten, A. Hansel, J. Curtius, Characterization of the mass-dependent transmission efficiency of a CIMS. *Atmos. Meas. Tech.* **9**, 1449–1460 (2016).
38. N. Hyttinen, O. Kupiainen-Määttä, M. P. Rissanen, M. Muuronen, M. Ehn, T. Kurtén, Modeling the charging of highly oxidized cyclohexene ozonolysis products using nitrate-based chemical ionization. *J. Phys. Chem. A* **119**, 6339–6345 (2015).
39. T. Berndt, S. Richters, T. Jokinen, N. Hyttinen, T. Kurtén, R. V. Otkjær, H. G. Kjaergaard, F. Stratmann, H. Herrmann, M. Sipilä, M. Kulmala, M. Ehn, Hydroxyl radical-induced formation of highly oxidized organic compounds. *Nat. Commun.* **7**, 13677 (2016).
40. F. D. Lopez-Hilfiker, C. Mohr, M. Ehn, F. Rubach, E. Kleist, J. Wildt, T. F. Mentel, A. Lutz, M. Hallquist, D. Worsnop, J. A. Thornton, A novel method for online analysis of gas and particle composition: Description and evaluation of a Filter Inlet for Gases and AEROsols (FIGAERO). *Atmos. Meas. Tech.* **7**, 983–1001 (2014).
41. D. Stolzenburg, L. Fischer, A. L. Vogel, M. Heinritzi, M. Schervish, M. Simon, A. C. Wagner, L. Dada, L. R. Ahonen, A. Amorim, A. Baccarini, P. S. Bauer, B. Baumgartner, A. Bergen, F. Bianchi, M. Breitenlechner, S. Brilke, S. Buenrostro Mazon, D. Chen, A. Dias, D. C. Draper, J. Duplissy, I. El Haddad, H. Finkenzeller, C. Frege, C. Fuchs, O. Garmash, H. Gordon, X. He, J. Helm, V. Hofbauer, C. R. Hoyle, C. Kim, J. Kirkby, J. Kontkanen, A. Kürten, J. Lampilahti, M. Lawler, K. Lehtipalo, M. Leiminger, H. Mai, S. Mathot, B. Mentler, U. Molteni, W. Nie, T. Nieminen, J. B. Nowak, A. Ojdanic, A. Onnela, M. Passananti, T. Petäjä, L. L. J. Quéléver, M. P. Rissanen, N. Sarnela, S. Schallhart, C. Tauber, A. Tomé, R. Wagner, M. Wang, L. Weitz, D. Wimmer, M. Xiao, C. Yan, P. Ye, Q. Zha, U. Baltensperger, J. Curtius, J. Dommen, R. C. Flagan, M. Kulmala, J. N. Smith, D. R. Worsnop, A. Hansel, N. M. Donahue, P. M. Winkler, Rapid growth of organic aerosol nanoparticles over a wide tropospheric temperature range. *Proc. Natl. Acad. Sci.* **115**, 9122–9127 (2018).
42. M. Breitenlechner, L. Fischer, M. Hainer, M. Heinritzi, J. Curtius, A. Hansel, PTR3: An instrument for studying the lifecycle of reactive organic carbon in the atmosphere. *Anal. Chem.* **89**, 5824–5831 (2017).
43. J. Vanhanen, J. Mikkilä, K. Lehtipalo, M. Sipilä, H. E. Manninen, E. Siivola, T. Petäjä, M. Kulmala, Particle size magnifier for nano-CN detection. *Aero. Sci. Technol.* **45**, 533–542 (2011).
44. K. Lehtipalo, J. Leppa, J. Kontkanen, J. Kangasluoma, A. Franchin, D. Wimnner, S. Schobesberger, H. Junninen, T. Petaja, M. Sipila, J. Mikkila, J. Vanhanen, D. R. Worsnop, M. Kulmala, Methods for determining particle size distribution and growth rates between 1 and 3 nm using the Particle Size Magnifier. *Boreal Environ. Res.* **19**, 215–236 (2014).
45. D. Stolzenburg, G. Steiner, P. M. Winkler, A DMA-train for precision measurement of sub-10 nm aerosol dynamics. *Atmos. Meas. Tech.* **10**, 1639–1651 (2017).
46. S. Mirme, A. Mirme, The mathematical principles and design of the NAIS—A spectrometer for the measurement of cluster ion and nanometer aerosol size distributions. *Atmos. Meas. Tech.* **6**, 1061–1071 (2013).
47. J. Kangasluoma, A. Samodurov, M. Attoui, A. Franchin, H. Junninen, F. Korhonen, T. Kurtén, H. Vehkamäki, M. Sipilä, K. Lehtipalo, D. R. Worsnop, T. Petäjä, M. Kulmala, Heterogeneous nucleation onto ions and neutralized ions: Insights into sign-preference. *J. Phys. Chem. C* **120**, 7444–7450 (2016).
48. K. Lehtipalo, L. Rondo, J. Kontkanen, S. Schobesberger, T. Jokinen, N. Sarnela, A. Kürten, S. Ehrhart, A. Franchin, T. Nieminen, F. Riccobono, M. Sipilä, T. Yli-Juuti, J. Duplissy, A. Adamov, L. Ahlm, J. Almeida, A. Amorim, F. Bianchi, M. Breitenlechner, J. Dommen, A. J. Downard, E. M. Dunne, R. C. Flagan, R. Guida, J. Hakala, A. Hansel, W. Jud, J. Kangasluoma, V.-M. Kerminen, H. Keskinen, J. Kim, J. Kirkby, A. Kupc, O. Kupiainen-Määttä, A. Laaksonen, M. J. Lawler, M. Leiminger, S. Mathot, T. Olenius, I. K. Ortega, A. Onnela, T. Petäjä, A. Praplan, M. P. Rissanen, T. Ruuskanen, F. D. Santos, S. Schallhart, R. Schnitzhofer, M. Simon, J. N. Smith, J. Tröstl, G. Tsagkogeorgas, A. Tomé, P. Vaattovaara, H. Vehkamäki, A. E. Vrtala, P. E. Wagner, C. Williamson, D. Wimmer, P. M. Winkler, A. Virtanen,

N. M. Donahue, K. S. Carslaw, U. Baltensperger, I. Riipinen, J. Curtius, D. R. Worsnop, M. Kulmala, The effect of acid–base clustering and ions on the growth of atmospheric nano-particles. *Nat. Commun.* **7**, 11594 (2016).
49. J. Kontkanen, T. Olenius, K. Lehtipalo, H. Vehkamäki, M. Kulmala, K. E. J. Lehtinen, Growth of atmospheric clusters involving cluster–cluster collisions: Comparison of different growth rate methods. *Atmos. Chem. Phys.* **16**, 5545–5560 (2016).
50. J. L. Fry, D. C. Draper, K. C. Barsanti, J. N. Smith, J. Ortega, P. M. Winkler, M. J. Lawler, S. S. Brown, P. M. Edwards, R. C. Cohen, L. Lee, Secondary organic aerosol formation and organic nitrate yield from NO_3 oxidation of biogenic hydrocarbons. *Environ. Sci. Technol.* **48**, 11944–11953 (2014).
51. N. L. Ng, S. S. Brown, A. T. Archibald, E. Atlas, R. C. Cohen, J. N. Crowley, D. A. Day, N. M. Donahue, J. L. Fry, H. Fuchs, R. J. Griffin, M. I. Guzman, H. Herrmann, A. Hodzic, Y. Iinuma, J. L. Jimenez, A. Kiendler-Scharr, B. H. Lee, D. J. Luecken, J. Mao, R. McLaren, A. Mutzel, H. D. Osthoff, B. Ouyang, B. Picquet-Varrault, U. Platt, H. O. T. Pye, Y. Rudich, R. H. Schwantes, M. Shiraiwa, J. Stutz, J. A. Thornton, A. Tilgner, B. J. Williams, R. A. Zaveri, Nitrate radicals and biogenic volatile organic compounds: Oxidation, mechanisms, and organic aerosol. *Atmos. Chem. Phys.* **17**, 2103–2162 (2017).
52. T. Berndt, W. Scholz, B. Mentler, L. Fischer, H. Herrmann, M. Kulmala, A. Hansel, Accretion product formation from self- and cross-reactions of RO_2 radicals in the atmosphere. *Angew. Chem. Int. Ed. Engl.* **57**, 3820–3824 (2018).
53. Y. Zhao, J. A. Thornton, H. O. T. Pye, Quantitative constraints on autoxidation and dimer formation from direct probing of monoterpene-derived peroxy radical chemistry. *Proc. Natl. Acad. Sci. U.S.A.* **115**, 12142–12147 (2018).
54. R. Atkinson, Rate constants for the atmospheric reactions of alkoxy radicals: An updated estimation method. *Atmos. Environ.* **41**, 8468–8485 (2007).
55. C. Yan, W. Nie, M. Äijälä, M. P. Rissanen, M. R. Canagaratna, P. Massoli, H. Junninen, T. Jokinen, N. Sarnela, S. A. K. Häme, S. Schobesberger, F. Canonaco, L. Yao, A. S. H. Prévôt, T. Petäjä, M. Kulmala, M. Sipilä, D. R. Worsnop, M. Ehn, Source characterization of highly oxidized multifunctional compounds in a boreal forest environment using positive matrix factorization. *Atmos. Chem. Phys.* **16**, 12715–12731 (2016).
56. T. Kurten, K. H. Møller, T. B. Nguyen, R. H. Schwantes, P. K. Misztal, L. Su, P. O. Wennberg, J. L. Fry, H. G. Kjaergaard, Alkoxy radical bond scissions explain the anomalously low secondary organic aerosol and organonitrate yields from α-Pinene + NO_3. *J. Phys. Chem. Lett.* **8**, 2826–2834 (2017).
57. J. F. Pankow, W. E. Asher, SIMPOL.1: A simple group contribution method for predicting vapor pressures and enthalpies of vaporization of multifunctional organic compounds. *Atmos. Chem. Phys.* **8**, 2773–2796 (2008).
58. S. Compernolle, K. Ceulemans, J.-F. Müller, EVAPORATION: A new vapour pressure estimation method for organic molecules including non-additivity and intramolecular interactions. *Atmos. Chem. Phys.* **11**, 9431–9450 (2011).
59. Y. Nannoolal, J. Rarey, D. Ramjugernath, Estimation of pure component properties: Part 3. Estimation of the vapor pressure of non-electrolyte organic compounds via group contributions and group interactions. *Fluid Phase Equilib.* **269**, 117–133 (2008).
60. T. Kurtén, K. Tiusanen, P. Roldin, M. Rissanen, J.-N. Luy, M. Boy, M. Ehn, N. Donahue, α-Pinene autoxidation products may not have extremely low saturation vapor pressures despite high O:C ratios. *J. Phys. Chem. A* **120**, 2569–2582 (2016).
61. Y. Li, U. Pöschl, M. Shiraiwa, Molecular corridors and parameterizations of volatility in the chemical evolution of organic aerosols. *Atmos. Chem. Phys.* **16**, 3327–3344 (2016).
62. T. Nieminen, K. E. J. Lehtinen, M. Kulmala, Sub-10 nm particle growth by vapor condensation—Effects of vapor molecule size and particle thermal speed. *Atmos. Chem. Phys.* **10**, 9773–9779 (2010).
63. T. F. Mentel, M. Springer, M. Ehn, E. Kleist, I. Pullinen, T. Kurtén, M. Rissanen, A. Wahner, J. Wildt, Formation of highly oxidized multifunctional compounds: Autoxidation of peroxy radicals formed in the ozonolysis of alkenes—Deduced from structure-product relationships. *Atmos. Chem. Phys.* **15**, 6745–6765 (2015).
64. B. H. Lee, C. Mohr, F. D. Lopez-Hilfiker, A. Lutz, M. Hallquist, L. Lee, P. Romer, R. C. Cohen, S. Iyer, T. Kurtén, W. Hu, D. A. Day, P. Campuzano-Jost, J. L. Jimenez, L. Xu, N. L. Ng, H. Guo, R. J. Weber, R. J. Wild, S. S. Brown, A. Koss, J. de Gouw, K. Olson, A. H. Goldstein, R. Seco, S. Kim, K. McAvey, P. B. Shepson, T. Starn, K. Baumann, E. S. Edgerton, J. Liu, J. E. Shilling, D. O. Miller, W. Brune, S. Schobesberger, E. L. D'Ambro, J. A. Thornton, Highly functionalized organic nitrates in the southeast United States: Contribution to secondary organic aerosol and reactive nitrogen budgets. *Proc. Natl. Acad. Sci. U.S.A.* **113**, 1516–1521 (2016).

Acknowledgments: We thank CERN for supporting CLOUD with technical and financial resources. We thank P. Carrie, L. P. De Menezes, J. Dumollard, K. Ivanova, F. Josa, I. Krasin, R. Kristic, A. Laassiri, O. S. Maksumov, B. Marichy, H. Martinati, S. V. Mizin, R. Sitals, A. Wasem, and M. Wilhelmsson for their contributions to the experiment. We thank the tofTools team for providing programs for data analysis of mass spectrometry. **Funding:** This research has received funding from the EC Seventh Framework Programme and European Union's Horizon 2020 programme (Marie Curie ITN no. 316662 "CLOUD-TRAIN," MSCA-IF no. 656994 "nano-CAVa," MC-COFUND grant no. 600377, and ERC project no. 692891 "DAMOCLES," no. 638703 "COALA," no. 257360 "MOCAPAF," no. 227463 "ATMNUCLE," no. 616075 "NANODYNAMITE," no. 335478 "QAPPA," and no.742206 "ATM-GTP"), the German Federal Ministry of Education and Research (project nos. 01LK0902A, 01LK1222A, and 01LK1601A), the Swiss National Science Foundation (project nos. 200020_135307, 206620_141278, 200021_140663, and 206021_144947/1), the Academy of Finland (Center of Excellence no. 1118615, project nos. 135054, 133872, 251427, 139656, 139995, 137749, 141217, 141451, 299574, 138951, 251007, 317380, 320094, and 316114), the Finnish Funding Agency for Technology and Innovation, the Väisälä Foundation, the Nessling Foundation, the Austrian Science Fund (FWF; project no. J3951-N36), the Austrian Research Funding Association (FFG, project no. 846050), the Portuguese Foundation for Science and Technology (project no. CERN/FP/116387/2010), the Swedish Research Council Formas (project no. 2015-749), Vetenskapsrådet (grant 2011-5120), the Presidium of the Russian Academy of Sciences and Russian Foundation for Basic Research (grants 08-02-91006-CERN and 12-02-91522-CERN), the U.S. National Science Foundation (grants AGS1136479, AGS1447056, AGS1439551, CHE1012293, AGS1649147, and AGS1602086), the U.S. Department of Energy (grant DE-SC0014469), the NERC GASSP project NE/J024252/1m, the Royal Society (Wolfson Merit Award), United Kingdom Natural Environment Research Council grant NE/K015966/1, Dreyfus Award EP-11-117, the French National Research Agency, the Nord-Pas de Calais, European Funds for Regional Economic Development Labex-Cappa grant ANR-11-LABX-0005-01, the National Natural Science Foundation of China, (D0512/41675145), and the Jiangsu Collaborative Innovation Center for Climate Change. M.S. acknowledges funding from the Academy of Finland (3282290) and H2020 European Research Council ERC-StG ("GASPARCON", 714621). **Author contributions:** C.Y., W.N., K.L., M.E., and M.K. designed the experiments and wrote the paper. C.Y., W.N., A.L.V., L.D., K.L., D.S., R.W., M.X., and C.R. analyzed the main datasets. All other authors contributed to the design of the facility, preparation of the instruments, or data collection and commented on the manuscript. **Competing interests:** The authors declare that they have no competing interests. **Data and materials availability:** All data needed to evaluate the conclusions in the paper are present in the paper and/or the Supplementary Materials. Additional data related to this paper may be requested from the authors. The datasets generated during and/or analyzed during the current study are available from the corresponding author on reasonable request.

Submitted 1 July 2019
Accepted 19 March 2020
Published 27 May 2020
10.1126/sciadv.aay4945

Citation: C. Yan, W. Nie, A. L. Vogel, L. Dada, K. Lehtipalo, D. Stolzenburg, R. Wagner, M. P. Rissanen, M. Xiao, L. Ahonen, L. Fischer, C. Rose, F. Bianchi, H. Gordon, M. Simon, M. Heinritzi, O. Garmash, P. Roldin, A. Dias, P. Ye, V. Hofbauer, A. Amorim, P. S. Bauer, A. Bergen, A.-K. Bernhammer, M. Breitenlechner, S. Brilke, A. Buchholz, S. B. Mazon, M. R. Canagaratna, X. Chen, A. Ding, J. Dommen, D. C. Draper, J. Duplissy, C. Frege, C. Heyn, R. Guida, J. Hakala, L. Heikkinen, C. R. Hoyle, T. Jokinen, J. Kangasluoma, J. Kirkby, J. Kontkanen, A. Kürten, M. J. Lawler, H. Mai, S. Mathot, R. L. Mauldin III, U. Molteni, L. Nichman, T. Nieminen, J. Nowak, A. Ojdanic, A. Onnela, A. Pajunoja, T. Petäjä, F. Piel, L. L. J. Quéléver, N. Sarnela, S. Schallhart, K. Sengupta, M. Sipilä, A. Tomé, J. Tröstl, O. Väisänen, A. C. Wagner, A. Ylisirniö, Q. Zha, U. Baltensperger, K. S. Carslaw, J. Curtius, R. C. Flagan, A. Hansel, I. Riipinen, J. N. Smith, A. Virtanen, P. M. Winkler, N. M. Donahue, V.-M. Kerminen, M. Kulmala, M. Ehn, D. R. Worsnop, Size-dependent influence of NO_x on the growth rates of organic aerosol particles. *Sci. Adv.* **6**, eaay4945 (2020).